Conformational plasticity modulates sequence specificity in non-canonical tandem RRM-RNA binding

Roxana Geanina Vasarhelyi [1,2], Vlad Cojocaru [1,2*]

[1]Doctoral School for Integrative Biology, Faculty of Biology and Geology, Babeş-Bolyai University, Cluj-Napoca, Romania

[2]Star-UBB Institute , Babeş-Bolyai University, Cluj-Napoca, Romania

Short title : Structural dynamics in tandem RRM - RNA binding

Keywords: RRM domain; RNA-binding proteins; conformational change; sequence specificity; molecular recognition; tandem RRM; molecular dynamics simulation

* Correspondence to:

Vlad Cojocaru

STAR-UBB Institute, Babeş-Bolyai University

Tiberiu Popoviciu street 2-4, Cluj-Napoca, Romania

Email: vlad.cojocaru@ubbcluj.ro

Web: https://cojocarulab.eu

Abstract

The Dead End protein, a key regulator of germline cell fate, utilizes two RNA Recognition Motifs (RRM) in tandem to bind AU-rich RNA in a non-canonical manner. Only one RRM uses the known RNA binding interface, whereas the second motif has only minimal contacts with the RNA. To characterize the structural features and dynamics that contribute to RNA binding, we performed a series of atomistic molecular dynamics simulations and show that the complex is highly flexible, undergoing large conformational transitions and deviating significantly from the initial experimental structure. We found that RNA binding significantly restricts but does not abolish the inter-domain movement of the two motifs, whereas the cooperative action of both RRM domains restricts RNA dynamics. Despite the extensive comformational plasticity of the complex, the core of the RNA binding interface and the sequence specificity is maintained. In the absence of one RRM, the RNA binding interface of the first RRM is extended whereas that of the second RRM is diminished leading to destabilization of the RRM-RNA interaction and even unbinding. This is in agreement with previous findings suggesting that the second RRM does not bind RNA on its own. The cooperative binding of the two RRMs is required for maintaining the core sequence specificity. These findings provide a paradigm shift towards considering highly dynamic RNA binding interfaces as key in RNA binding and regulation.

Introduction

RNA-binding proteins (RBPs) are key regulators of gene expression. They interact with RNA to form ribonucleoprotein (RNP) complexes [1,2]. Most RBPs contain at least one RNA Binding Domain (RBD) [3], which allows them to control nearly all steps of RNA processing [4,5]. The RNA Recognition Motif (RRM) is the most common RBD in eukaryotes [2]. Found in over 50% of human RBPs, with the human genome encoding 239 proteins that have at least one RRM domain [6], this prevalence highlights its critical role in post-transcriptional gene regulation (PTGR) by recognizing single-stranded RNA (ssRNA) [3].

The RRM fold is highly conserved [7], but it is also functionally versatile in its role in gene regulation. Its core structure, established through high-resolution studies [8–12], is defined by a canonical $\beta_1\alpha_1\beta_2\beta_3\alpha_2\beta_4$ topology, consisting of four β-strands and two α-helices [3]. Canonical RRM binding happens on the central β sheet [3] and is controlled by two key consensus sequences: RNP1 on the β_3 strand and RNP2 on the β1 strand [1,3–5]. These sequences bare aromatic amino acids which form sequence-specific interactions with the RNA bases [4]. While a single RRM can bind up to eight nucleotides, multiple RRM domains often work together to increase binding specificity affinity [13].

Tandem RRM proteins exhibit diverse inter-domain orientations that determine their cooperative RNA binding mode, requiring the domains to either bind adjacent RNA sites or recognize sites

separated by an RNA loop [14]. Some RRMs deviate from this standard structure, exhibiting non-canonical features such as additional α-hairpins [15] or β-sheets [16,17].

An important example of such a protein is Dead end protein (DND1), which consists of two RRMs and a Double-Stranded RNA Binding Domain (dsRBD) [18,19]. As an essential, conserved RBP, DND1 is critical for maintaining primordial germ cell (PGC) fate and survival [20–22], where its loss is directly linked to the formation of germ cell tumors [23]. Structural analysis of its non-canonical RRMs (PDB: 7Q4L) revealed an unusual cooperative binding mechanism for high-affinity recognition of the AU-rich consensus sequence [18]. The two RRM domains, RRM1 and RRM2, cooperate to achieve high-affinity binding to AU-rich RNA targets. RRM1 is the essential primary binding platform due to its extended RRM (eRRM) fold and, together with the ultra-short interdomain linker, mediates the sequence-specific recognition of a central adenosine (A4) residue in the RNA. In contrast, the non-canonical RRM2, which lacks aromatic RNP residues and does not bind RNA alone, acts as a stabilizing lock. It achieves this by using an atypical binding pocket on its α-helix 2 to specifically recognize a uridine (U6) residue and cap the RNA, forcing an unusual 120° turn in the RNA backbone and increasing the overall binding affinity [24].

Functionally, DND1 serves as a dual regulator, capable of stabilizing target transcripts by blocking microRNA (miRNA) access [24], or conversely, promoting decay by recruiting the CCR4-NOT (C-C Chemokine Receptor 4-Negative On TATA-less) deadenylation complex, a mechanism dictated in part by the protein's dsRBD [22]. These opposing regulatory functions are central to its involvement in disease, as confirmed in a systematic review by Faraji et. all [23]: DND1's stabilizing role promotes anti-cancerous effects in some somatic cells, e,g. by stabilizing pro-apoptotic mRNA, whereas its repressive function, via CCR4-NOT recruitment, is linked to tumor formation when deregulated [18,24]. In development, DND1 partners with the NANOS3 (NANOS homolog 3) protein to suppress translation of genes such as SOX4, thereby constraining germ cell lineage specification [25]. Furthermore, while DND1 can act as a tumor suppressor in some somatic contexts [26], recent discoveries show a pro-tumorigenic role in melanoma, where the circular RNA binds directly to DND1, sequestering it and reversing its inhibitory effect on the PI3K/AKT (Phosphoinositide 3-kinase/protein kinase B) signaling pathway , thereby positioning the circular RNA as a potential diagnostic biomarker and therapeutic target [27].

Despite the availability of one experimental structure for the non-canonical DND1 RRM-RNA complex (PDB: 7Q4L), the role of conformational plasticity in this cooperative tandem RRM - RNA recognition mechanism remains unknown. We present here extensive molecular dynamics simulations of the DND1 tandem RRM-RNA complex, the RRM–RNA complexes of the individual RRMs and the apo protein and RNA. From these we found that the complex is highly flexible deviating significantly from the experimental structure. RNA binding restricts but does not abolish the inter-domain motion of the two RRMs. At the same time, the cooperative tandem RRM-RNA binding restricts the conformational plasticity of the RNA. Despite this conformational plasticity, the core RNA binding interface and sequence specificity is maintained in the tandem

RRM-RNA complex. Remarkably, from the simulations of the RRM-RNA complexes for each individual RRM, we found that the cooperative binding of the two RRMs is required for maintaining the interactions that define the core sequence specificity. In agreement with previous experiments, the RRM1-RNA but not the RRM2-RNA interface remains stable during these simulations.

Methods

Structure prediction with AlphaFold 3

We generated a total of 25 predicted structures for the protein-RNA complex by running 5 predictions using the AlphaFold 3 (AF3) server [28],each with a different seed number (resulting in five models per prediction). We selected the top five models from the complete set based on the highest pLDDT (predicted Local Distance Difference Test) scores, a measure of structural confidence. We assessed the quality and accuracy of these chosen models using a CAPRI-based [29] analysis performed by HADDOCK3[30], using the complex's NMR (nuclear magnetic resonance) ensemble (PDB: 7Q4L)[18] as the reference experimental structure for validation. We quantified model performance using the Interface Root Mean Square Deviation (IRMSD), which measures backbone atom deviation exclusively at the protein-RNA interface, and the Fraction of Native Contacts (FNAT), which reports the percentage of residue-residue contacts from the reference reproduced by the predicted structure (Table S1). We used these metrics to quantify the deviation of the AF3 predicted structures from the experimental reference, noting that the PDB entry for the experimental structure was within the AF3 training data.

Modelling the systems for molecular dynamics simulations

From the experimental structure PDB 7Q4L [18] which contains an ensemble of 20 structures derived from NMR data, three frames were selected (Figure S1), each exhibiting slightly different conformations: two having the N-terminal extension (from G1 to N7) of RRM1 away from the globular domain but in different orientations, and one where it is closer to the RRM1 and the RNA binding site. The details of each system's configuration can be found in Figure S1. To better reflect the natural environment of the protein in which the RRMs are not isolated, we generated models of DND1 with extended terminal tails using Modeller [31]. For this we added 10 amino acids to the N-terminal tail and 8 amino acids to the C-terminal tail. To build the models, we used the selected structures from the 7Q4L ensemble as templates and aligned the DND1 protein sequence on it (UniProt ID: Q8IYX4)[32] (Figure S2).

To study the role of each RRM in RNA binding, we prepared for simulations truncated models which contain only one RRM bound to the RNA (RRM1-RNA and RRM2-RNA) simply by removing the other RRM. Furthermore, we prepared models of the unbound tandem RRMs (RRM1-RRM2) and unbound individual RRMs (RRM1 and RRM2). In this way we obtained a total of 21 models (Table S2) for the follow-up MD simulations.

Molecular dynamics simulations

We established a total of seven molecular systems for MD analysis: the full DND1-RNA (RRM1-RRM2-RNA) complex, the RRM1-RRM2 tandem domain, RRM1-RNA, RRM2-RNA, RRM1, RRM2, and the RNA component. We performed three replicate simulations (M1, M2, and M3) for every system, totaling 21 simulations. We used a short 5 Å buffer distance between the solute and the edge of the water box. This distance works because the extended N-terminal and C-terminal tails make the box size large enough. We solvated the systems using the OPC water model [33] neutralized by the addition of appropriate counterions, Na^+ and Cl^- . Subsequently, both K^+Cl^- and Na^+Cl^- were added, each to an independent concentration of 100 mM. The protein and RNA parameters were assigned using the AMBER ff19SB force field [34] and the OL3 RNA force field [35], respectively. We optimized the solvated systems by energy minimization with the AMBER software [36]. Equilibration was carried out under constant temperature and pressure using NAMD [37]. The equilibration consisted of 17 sequential steps, totaling 4.875 ns, with parameters detailed in Table S3. The protocol systematically reduced positional restraints across the steps, beginning with restraints on all solute atoms and gradually removing them until the final unrestrained steps (Table S3). Temperature was maintained at 300 K using Langevin dynamics with a damping coefficient of 1 ps^{-1}, and pressure was controlled at 1 atm using the Langevin piston method detailed in Table S3. Short-range nonbonded interactions were truncated at 9 Å cutoff, and long-range electrostatics were computed using the Particle Mesh Ewald (PME) method. Molecular Dynamics (MD) simulations were performed in the isothermal-isobaric (NPT) ensemble for 1 us with a timestep of 2 fs. The temperature was kept constant at 300 K using Langevin dynamics with a damping coefficient of 0.1 ps. The pressure was maintained at 1 atm using the Langevin Piston method, with a piston period of 1.5 ps and a decay time of 1.2 ps, respectively. All simulations were performed with NAMD. Snapshots were selected for analysis every 5 ps.

Analysis of MD simulations

We processed the trajectories by imaging all molecules into the central unit box and anchoring the structural part (excluding the added extended tails residues 1-8 and 234-242) of each system. For faster analysis, we generated trajectories and topology files by removing the water box and the ions. To quantify the conformational flexibility, we calculated the Root Mean Square Fluctuation (RMSF) using all heavy atoms (non-hydrogen atoms) and averaging per residue. The RMSF was determined for the trajectory of each replicate (M1, M2, M3) individually, rather than by using a single ensemble average. We calculated Root Mean Square Deviations (RMSD) relative to the average coordinates of the 20 experimental NMR structures. For all protein-containing systems, we performed the fit on the structural core of the protein (excluding the added extended tails residues 1-8 and 234-242) to factor out translational and rotational motion. By default, this fit was performed either on the RRM1 or on the RRM2 domain to emphasize the motion of the RRMs relative to each other. For the simulation involving RNA, we performed the fit on the entire RNA molecule.

Furthermore, the distance between the center of mass (COM-COM) of the two RRMs and the radius of gyration (RoG) were calculated using CPPTRAJ (34) using only the structural regions of the domains (excluding the added extended tails residues 1-8 and 234-242), to capture the motion of the RRMs towards each other and their compactness.

To analyze the protein-RNA interactions in our simulations, we first generated contact maps using the 20 NMR frames as an experimental reference. Subsequently, we performed a detailed protein-RNA contact analysis on the simulated systems. For this analysis, two sets of maps were created: one focusing on contacts with the RNA backbone atoms (nonspecific contacts), and another on contacts between the RRMs and the RNA bases (specific contacts). We defined a contact as any pair of heavy atoms between protein and RNA that were found within 4.5 Å of each other. We used this distance cutoff to identify stable (present in more than 50 % of simulation), near-native interactions for both the specific and nonspecific contact analysis.

We calculated the surface accessible solvent area (SASA) for the β-sheets of RRM1, by selecting the β-sheet residues (32-36, 38-42, 58-62, 84-91, 97-105) and using the surf command in cpptraj. For the RRM2 calculation we selected the β-sheet residues (137-142, 166-170, 178-185, 211-214).

K-Means Clustering

To analyze the major conformational states sampled during the simulation, we performed k-means clustering using the cpptraj module of the amber software package. We reduced the size of the dataset by considering only one out of every ten frames (10%) from the trajectories, resulting in an effective time interval of 50 ps between consecutive analyzed frames. This identical sampling procedure was applied to all k-means clustering analysis. We clustered these selected frames into 10 distinct clusters based on an RMSD metric [38].

For the protein-containing systems, we calculated the RMSD over the Cα of the structural part of the protein (excluding flexible tails). For the RNA-alone simulations, we calculated the RMSD over all heavy atoms of the RNA molecule. K-means clustering partitions the MD frames into k clusters by minimizing the variance within each cluster, allowing us to identify the major conformational ensembles sampled.

Results

The DND1-RNA complex displays extensive conformational plasticity

The experimental structure of the DND1-RNA complex, determined by NMR spectroscopy shows 20 snapshots of the protein-RNA bound complex. The average structure of the DND1 protein illustrates the secondary structure elements of the two tandem RRMs, detailing the orientations of the β-strands and α-helices, and the overall relative orientation of RRM1 and RRM2 (Figure 1A). The structural differences observed across the NMR ensemble are mostly confined to the N-terminal and C-terminal extensions (Figure 1B).

A comparison of the experimental data with 25 models generated by AlphaFold3 (AF3) resulted from 5 independent runs with different random number seeds, shows that these predicted structures are significantly different from the experimental NMR structures (Figure 1C). In the analysis of the AF3 models we observe a range of values for the fraction of native contacts (FNAT) at the binding site (from 0.018 to 0.38). The FNAT values combined with high global and interface RMSD (IRMSD) values confirmed that the predicted models differ significantly from the experimental structure (Table S1).

Given these differences and the non-canonical nature of the DND1-RNA interaction, we performed MD simulations to understand the dynamics of the complex. We found that the complex samples many different conformations, most of them different from those found in the initial experimental structure (Figure 1D, E, F). To measure the flexibility, we calculated the RMSF and found that the RRM1 domain is less flexible than the RRM2 domain in 2 out of 3 DND1-RNA simulations. However, in one simulation (M3), the RRM2 domain fluctuated significantly less than in the other two (Figure 1G). Taking a look at the flexibility of the RNA (C1,U2,U3,A4,U5,U6,U7,G8) in simulations, we find that the central adenine nucleotide in the RNA (A4), which is known from experimental data to be important for binding, was less flexible than other RNA nucleotides in all 3 DND1-RNA simulations (Figure 1H).

Therefore, we show that the DND1-RNA complex displays extensive conformational plasticity in the simulations, which explains the inability of AlphaFold3 to predict the conformation observed in the NMR structure. The flexibility is largely driven by changes in the relative orientation of RRM2 domain towards RRM1 (Figure 1G), yet the essential central adenine nucleotide in the RNA and to some extent the two flanking U bases remain more rigid, confirming the sequence-specific binding of DND1 to a UAU triad (Figure 1H).

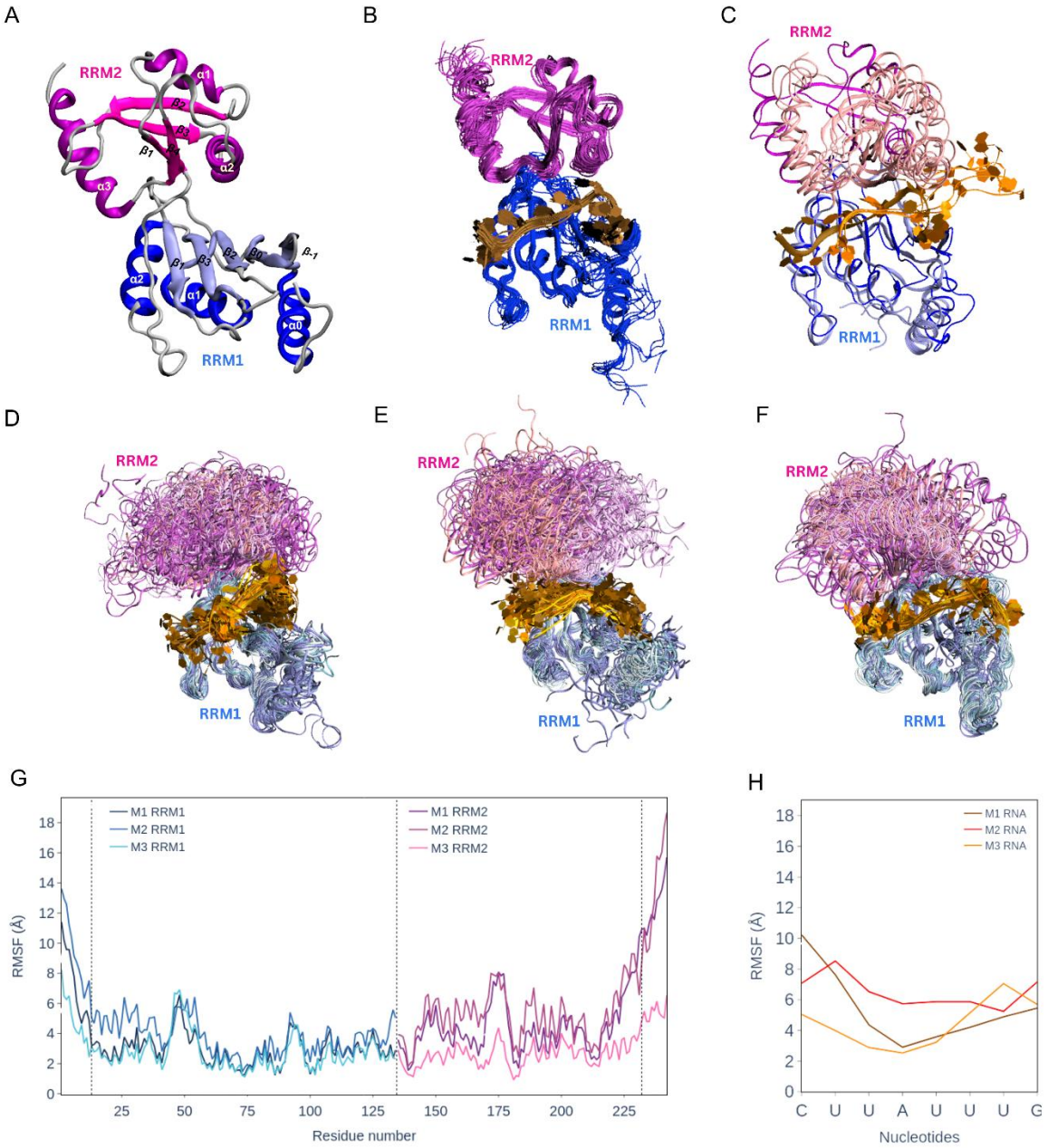

Figure 1. **Flexibility of the DND1-RNA complex during MD simulations.** (A) Secondary structure of the average structure of the DND1 protein from the NMR ensemble (PDB-ID 7Q4). (B) 20 structures from the experimental NMR ensemble (PDB: 7Q4L) superimposed. (C) 5 best AF3 models superimposed on the average experimental structure. Each model was the 1st ranked in each of the 5 runs with different random number seeds. (D-F) Snapshots of the entire simulation taken every 500 ps from simulations M1, M2, and M3. (G) RMSF of the protein across the ensemble of 3 simulations shows DND1 flexibility when bound to RNA (RRM1 in blue, RRM2 in pink). (H). RMSF of the RNA across the three simulations. The colors will be kept throughout this manuscript.

RNA binding restricts the inter-domain motion of the two RRMs

From the simulations of the DND1-RNA complex, we calculated the RMSD of the entire protein when fitting RRM1-RRM2 (no tails) and find that the complex deviates significantly from the starting experimental structure, exploring a wide range of conformations. To characterize this conformational landscape, we performed K-means clustering and recorded 10 clusters. When we superimposed on the cluster representative structures, on RRM1 we observe large changes in the orientation of RRM2 relative to RRM1. Analysis of the cluster representatives (Figure 2A) highlights the distinct range of orientations the two RRMs explore during the DND1-RNA simulations. The most populated cluster (cluster 0) represents conformations closest to the reference structure, primarily showing RRM2 slightly shifting from the RNA interface. Beyond this reference state, the less populated clusters capture two major types of dynamics. Inter-domain rotation is evident in cluster 1, where the α1 helix of RRM2 rotates away from the RNA while the entire RRM2 domain moves closer to RRM1. Simultaneously, we observe intra-domain changes within RRM2 itself: cluster 2 shows the RRM2 terminal tail and the α3 helix moving away from the RRM2 β-sheet (suggesting an open conformation), while cluster 5 presents a contrasting, enclosed conformation where the α3 helix and terminal tail move closer to the β-sheets. The remaining conformations, such as those in clusters 4 and 6, generally depict RRM2 slightly moving away from the RNA. Furthermore, the COM-COM distances highlight that the two domains were generally further apart from each other than in the experimental structure.

Next, we want to understand how the bound RNA modulates this conformational plasticity. For this, we performed the same RMSD and COM-COM distance calculations on the RRM1-RRM2 (apo-protein) system for comparison. The conformational changes in the apo-protein are more extensive, and the structures deviates even further from the experimental data, consistent with the RMSD values (Figure 2B). The cluster analysis reveals distinct categories of inter-domain motion explored by the RRM1-RRM2 system. The representative structure of cluster 7 has the conformation closest to the experimental structure. Beyond this reference, the most populated cluster, cluster 0, shows a rotational shift where the RRM2 α3 helix faces RRM1, resulting in a slightly greater distance between the domains. In contrast, cluster 1 captures an enclosed orientation, where RRM2 moves almost entirely on top of RRM1 with a significant decrease in inter-domain distance (Figure 2B). Cluster 2 also exhibits RRM2 rotation with the α3 helix toward RRM1, but here the entire RRM2 domain comes closer to RRM1. Further rotational diversity is seen in cluster 3, which involves RRM2 rotation coupled with a different intra-domain conformation. Finally, cluster 5 captures a more open state with a slight increase in the distance between the two domains (Figure 2B).

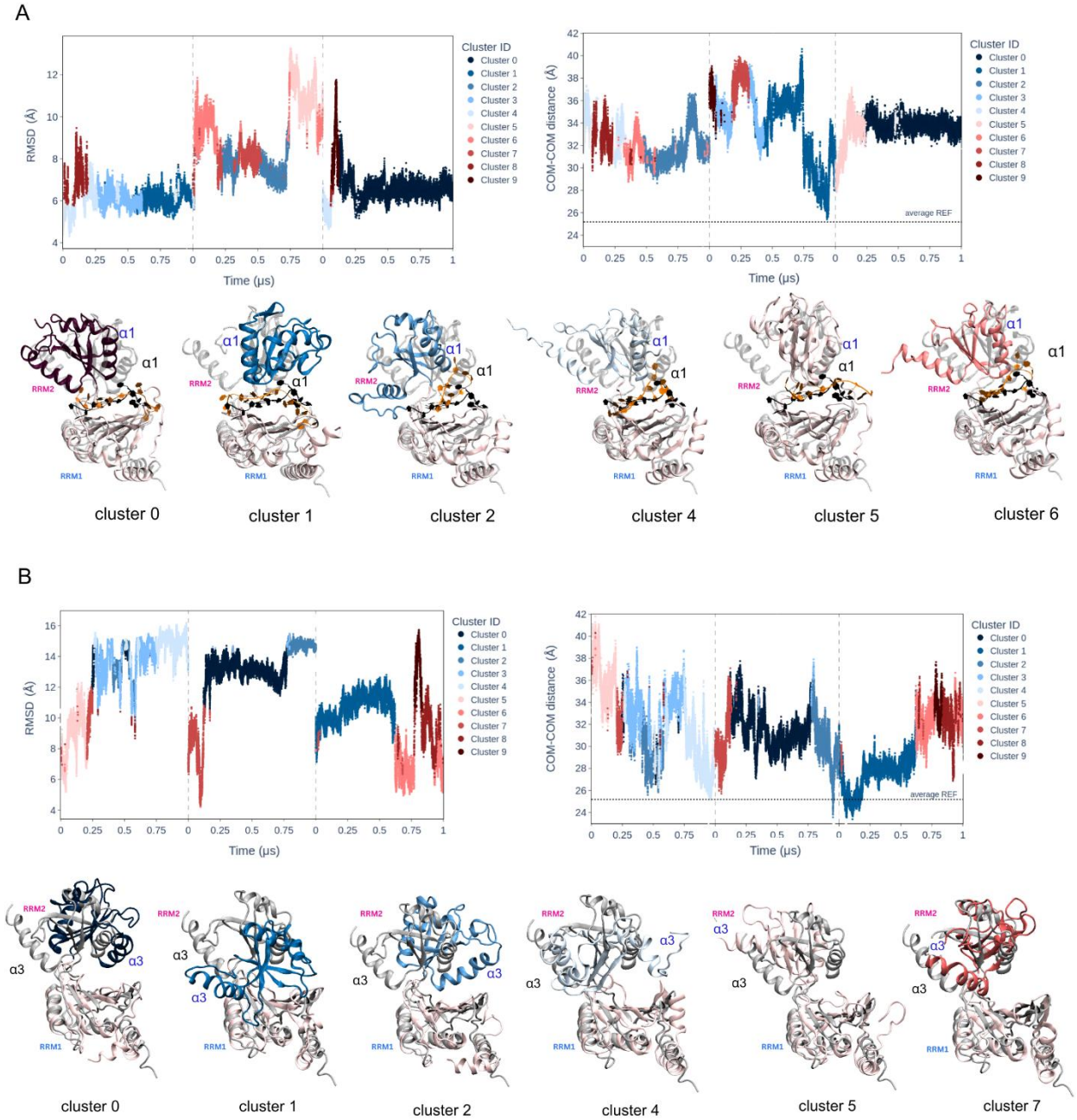

Figure 2. Intramolecular dynamics of the tandem RRMs. (A) when bound to RNA. (B) in free form. Each panel shows the RMSD (upper row left), the COM-COM distance (upper row right) and cluster representative structures (lower row) of the 6 most populated clusters. All data points and structures are color-coded by RMSD-based clustering to depict the dominant conformations and their diversity.

The clustering analysis shows that the RNA-free system is highly dynamic, spanning a broader range of conformations with the two protein domains moving both closer and further from each

other. These findings show that RNA binding restricts the inter-domain movement of the two RRM domains.

Cooperative binding of the two RRM domains restricts RNA dynamics

Following our analysis of the relative RRM domain motion, we performed two sets of RMSD calculations to determine how the dynamics of the RNA are modulated by its binding to the tandem RRMs (Figure 3). First, to study how the RNA dynamics are affected by binding to RRM1, we analyzed the RMSD of the RNA after fitting only the heavy atoms of RRM1 in the simulations of the DND1-RNA and RRM1-RNA systems (Figure 3A). The deviation of the RNA from the initial experimental structure is larger when RRM1 was bound alone to the RNA than when RRM1 and RRM2 were bound in tandem (Figure 3A).

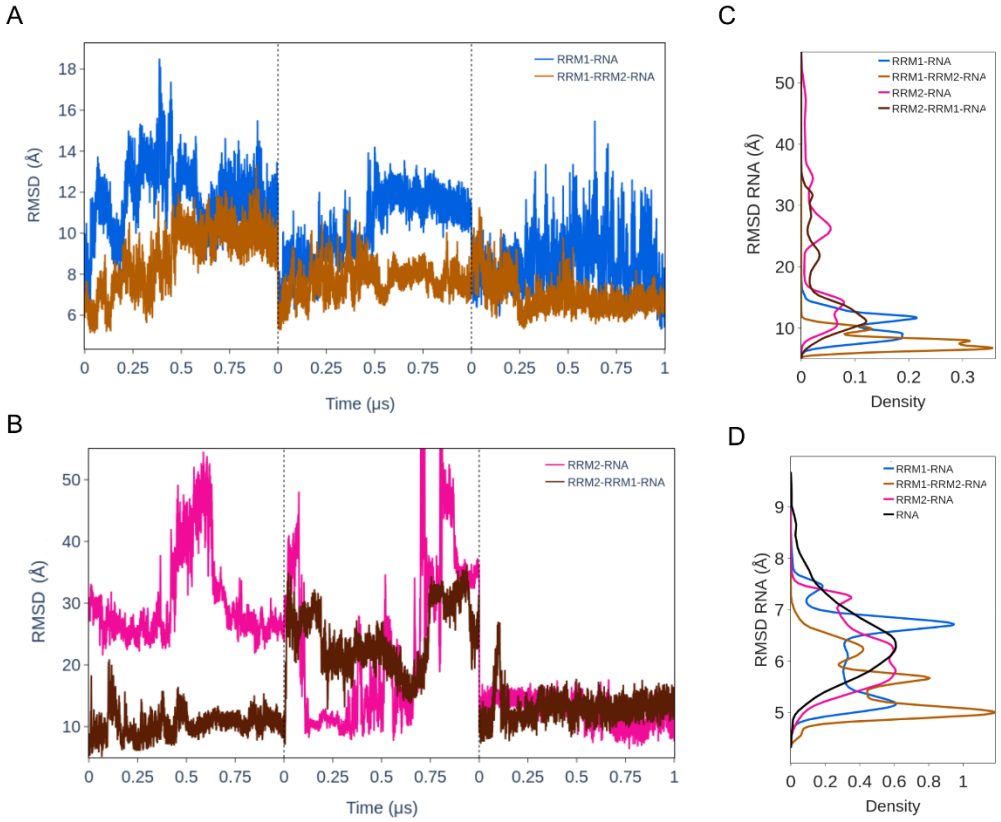

Figure 3. **RNA motion is relative to RRM1 and RRM2.** (A) RNA RMSD relative to RRM1 (fit on RRM1), comparing RRM1-RNA (blue) and DND1-RNA (brown) systems. (B) RNA RMSD relative to RRM2 (fit on RRM2), comparing RRM2-RNA (magenta) and RRM1-RRM2-RNA (dark brown) systems. (C) A combined histogram of the RNA RMSDs from all systems, summarizing RNA mobility (by fitting RRM1 in RRM1-RNA, RRM1-RRM2-RNA, and fit on RRM2 in RRM2-RNA, RRM2-RRM1-RNA systems). (D) RMSD histogram of all systems with RNA, by fitting the RNA to the average of the RNA from the experimental structure (apo RNA in black

Second, we calculated the RMSD of the RNA after fitting only the heavy atoms of RRM2 in the DND1-RNA and RRM2-RNA systems (Figure 3B). The significantly higher RMSD values in the DND1-RNA system here reflect the motion of RRM2 relative to RRM1. In addition, the RNA conformation deviates significantly more from the initial structure when bound to RRM2 alone than when bound to RRM2 in tandem with RRM1. Therefore, the RNA dynamics are restricted in the DND1-RNA system and both RRMs contribute to this, highlighting the cooperative binding. Interestingly, the RRM2-RNA system is more dynamic than the RRM1-RNA system, with RRM2-RNA being highly mobile in both M1 and M2 simulations. In the M2 simulation the RNA unbinds from RRM2 in the M2 simulation. Notably, in the M3 simulation the RRM2-RNA complex adopts a more stable conformation different from the experimental structure (Figure 3B).

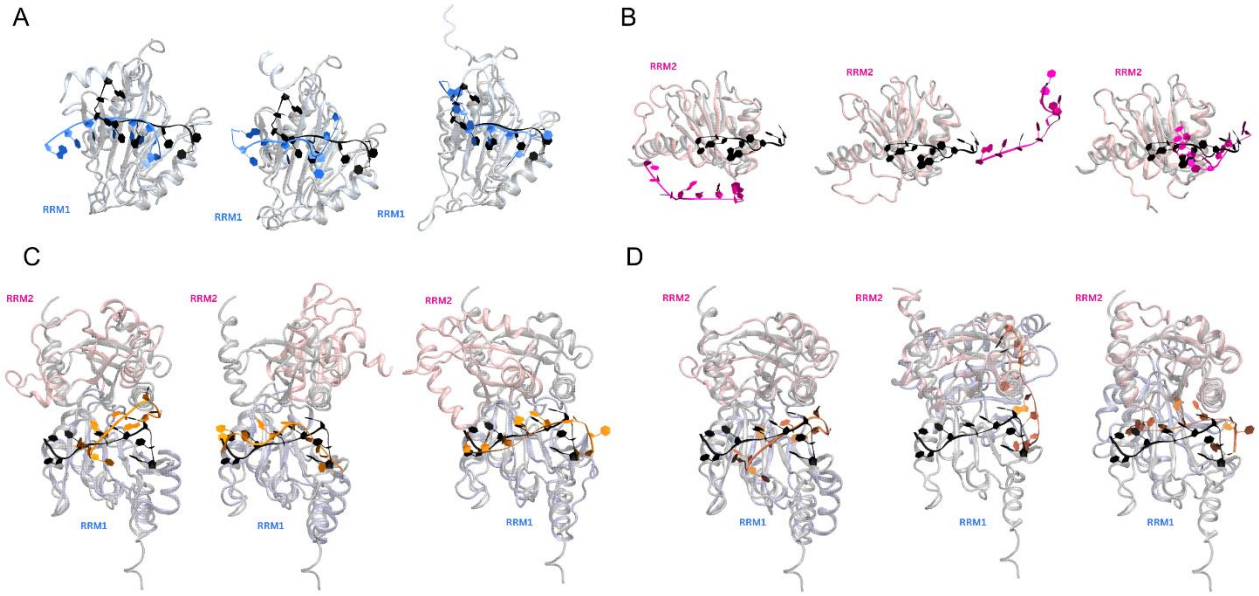

Figure 4. Structural snapshots illustrate RRM-RNA complex dynamics. Representative structures at the end of the simulations are shown. (A) RRM1-RNA complex, (B) RRM2-RNA complex, (C) RRM1-RRM2-RNA complex aligned on RRM1. (D) RRM1-RRM2-RNA complex aligned on RRM2. The coloring is kept from Figure 1.

Next, we analyzed the RMSD distributions from two distinct alignments. For the first histogram, the fit was applied to the protein (RRM1 fitted for the first 2 in legend and RRM2 for the last two), measuring the positional deviation of the RNA relative to the experimental structure (Figure 3C). The RMSD distribution for the RRM2-RNA system is significantly wider than for the RRM1-RNA system, indicating that the RNA exhibits a much broader range of structural displacement (or mobility) when bound to RRM2. The second histogram directly addresses the RNA's intrinsic shape change by calculating the RMSD for all the systems with the RNA including apo-RNA, with the fit applied to the RNA itself. This analysis shows the conformational differences induced by the isolated domains: the RRM1-RNA distribution has two distinct peaks, suggesting RRM1 enables two distinct RNA conformations during binding (one consistent with the experimental

structure and one further away), whereas the RRM2-RNA distribution closely resembles the behavior of the apo-RNA, indicating that RRM2 alone does not substantially change the intrinsic conformation of the RNA

Comparison of structural dynamics reveals differences between the RRM systems (Figure 4). In the RRM1-RNA system, small conformational changes indicate relatively stable binding. In contrast, the structures of the RRM2-RNA system sampled in simulation M2 reveal the RNA is unbinding from RRM2. Structural representations confirm that in the DND1-RNA simulation M2, the RRM2 domain rotates and moves away from the RNA, while the RNA remains anchored to the binding interface of RRM1.

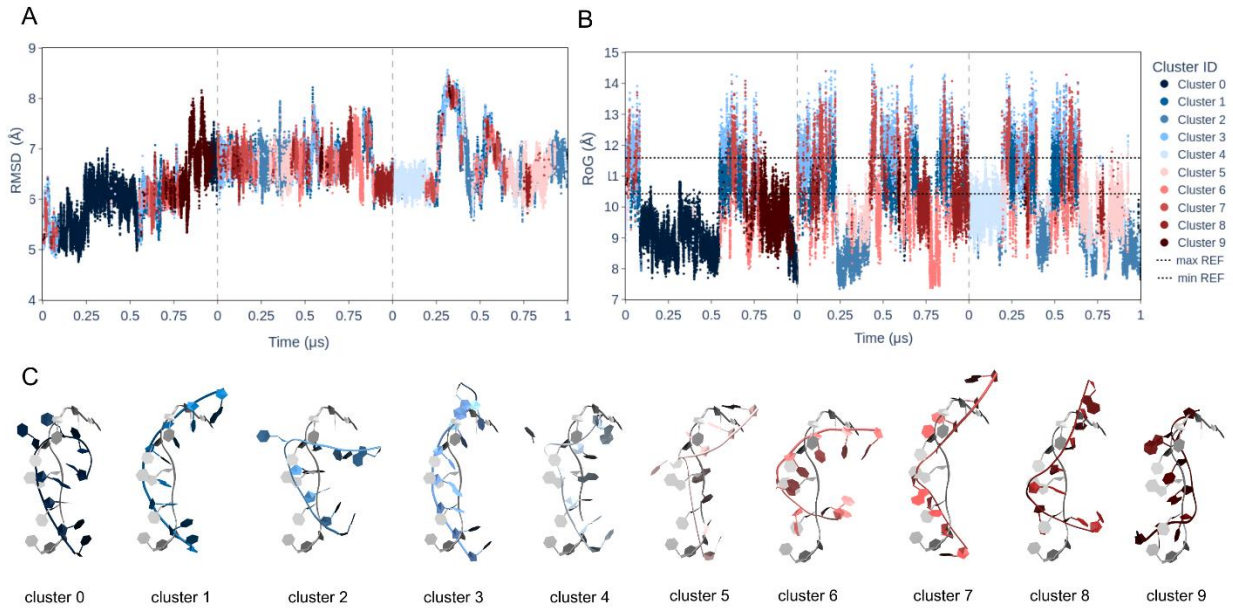

Figure 5. Conformational dynamics of free RNA in MD simulations. (A) RMSD. (B) Rog of the RNA over three 1-μs simulations show its overall stability and transitions between compact and extended conformations. (C) Representative structures from 10 clusters highlight the diversity of sampled conformations. All panels are colored by RMSD-based clustering of RNA structures to link conformational states with their metrics.

To understand how the dynamics of the RNA bound either to a single RRM or to both RRMs in tandem differ from the inherent conformational plasticity of the free RNA, we analyzed the simulations of the free RNA molecule. We calculated the RMSD of the RNA heavy atoms and Rog across three independent simulations. To understand the range of conformations sampled by the RNA in solution, we performed K-means clustering, and the 10 cluster representatives are shown in Figure 5. The Rog analysis confirms the RNA spans a variety of conformations, from compact to extended, including states within the Rog range of the experimentally bound structure (Figure 5B). The cluster representatives, when fitted against the kinked experimental conformation

of the bound RNA (PDB ID: 7Q4L), illustrate this conformational diversity (Fig 5C). For example, clusters 2 and 6 display more compact, closed conformations. Cluster 9 is particularly notable as its conformation closely resembles the kinked bound form, indicating that this kinked structure is accessible and stable in the unbound state. Conversely, clusters 1 and 7 represent more elongated, open conformations.

Core RRM-RNA interaction interface remains accessible in the absence of the RNA

Next, we asked whether the conformation of each RRM, bound to RNA alone or in tandem is also selected via conformational selection or rather established via an induced fit mechanism. To answer this, we analyzed the accessibility of the classical RRM-RNA interfaces (the β-sheets of the RRMs) by calculating the SASA of the β-sheet during the simulations. It is important to note that the DND1 binds RNA non-canonically, only the RRM1 establishing canonical interactions involving the β-sheet. The β-sheet SASA distributions of the RNA-bound RRM1 (Figure 6A) show density peaks at lower values than the experimental range, indicative of a lower accessibility of the sheet. The reduced SASA values in the DND1-RNA and RRM1-RNA systems, when compared to the experimental structure, provide evidence for an intrinsic closing mechanism of the two RRM domains over the bound RNA.

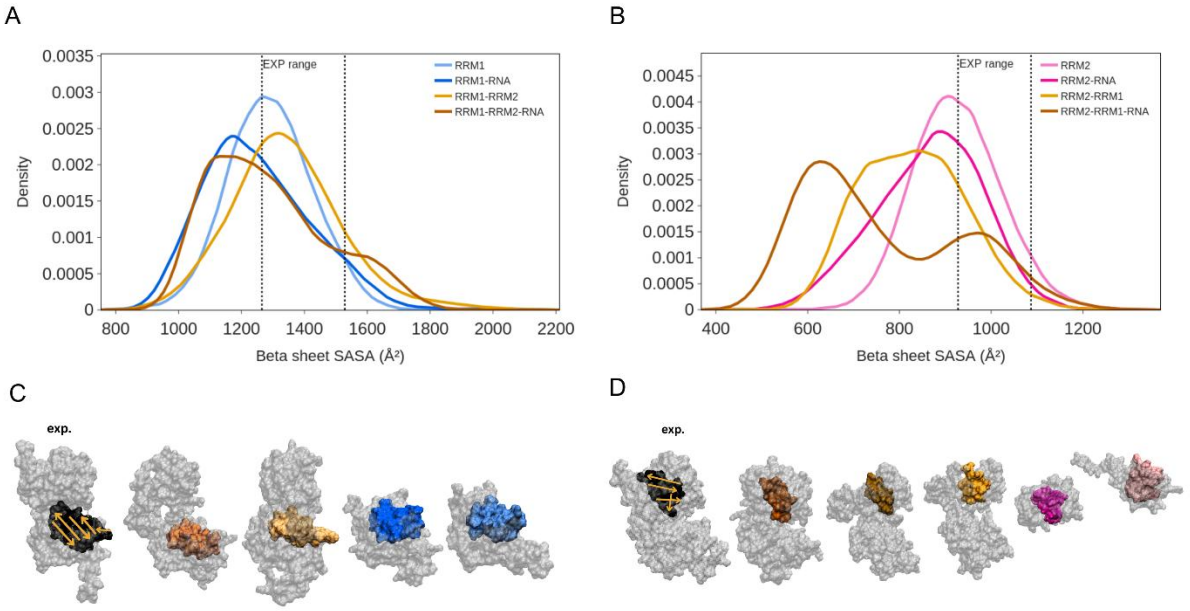

Figure 6. SASA calculation of the β-sheets in RRMs. (A-B) SASA of the β-sheet regions in RRM1 (A) and RRM2 (B), respectively. (C-D) Structural representations correspond to peak SASA values of RRM1 (C) and RRM2 (D), illustrating changes in β-sheet exposure. The first structure in black is the experimental NMR (PDB: 7Q4L) with the β-sheets represented as arrows on top of the surface.

In contrast, the β-sheet of RRM2 has only 4 β-strands and therefore the SASA values are lower compared to those seen for RRM1 which has 5 β-strands. In the DND1-RNA complex, the β-sheet of RRM2 has a distinct SASA distribution with two peaks, one of which falls directly within the range found in the experimental structures. Similar to RRM1, the distribution peaks for apo-RRM2 β-sheet SASA fall within the range found in the experimental values, but the difference between the distributions obtained from the simulations with apo and RNA-bound RRMs is smaller (Figure S3). In the full DND1-RNA complex, the RRM2 β-sheet SASA values are lower than in the RRM2 and RRM2-RNA systems, indicating that the presence of RRM1 has a more pronounced impact on the accessibility of the RRM2's β-sheet than the RNA binding.

Therefore, our findings indicate that the sidechains of amino acids known to be important for canonical RNA binding located on the surface of the β-sheets of the two RRMs are accessible for RNA binding in the apo form and that the presence of the other RRM domain does not restrict the accessibility of the RNA.

Core specific protein-RNA interactions are not affected by structural dynamics

To investigate whether the conformational plasticity driven by the orientational dynamics between the two RRMs affects the binding interface of the DND1-RNA complex, we performed a detailed contact analysis comparing the interfaces of our three MD simulations (M1, M2, M3) against the experimental reference structure. We first determined the native contacts from the 20-structure experimental ensemble of the DND1-RNA complex (PDB:7Q4L) (Figure S4). The native contacts, determined experimentally from a previous structural study (17), are defined by the key residues involved in stabilizing the complex: the RRM1 domain and linker anchor the central adenosine (A4) via stacking on F61 and F100 and sequence-specific recognition by linker residues (R133, S134, T135), while the RRM2 domain stabilizes this binding using its α-helix 2 pocket to provide sequence-specific recognition of U6 via a double hydrogen bond from K196 and W215 (17).

We observed that in the M1 simulation M1, the DND1-RNA interface was the most similar to that in the experimental structure, matching both specific and non-specific interactions. The main canonical interactions were stable, notably the A4 base stacking on F61 and F100 in the RRM1 domain. The linker-binding interface was maintained, even though we observed a slight shift in contacts established by A4 and U5. We attribute this stability to the RRM2 binding interface being stable, as it anchors the U6 nucleotide via sequence-specific contacts involving K196 and W215.

In the simulation M3, the core interface was also maintained similar to the reference, though with some key differences. We see that the canonical RRM1 interface is preserved, marked by the high-frequency stacking of A4 on F61. Interestingly, the RRM2 contacts show lower occupancies than in the M1 simulation, suggesting increased local dynamics. Remarkably, we found that a new and stable interaction involving H189 and U5 contributes to RRM2 stability. In the M3 simulation an extended binding interface was observed for the G8 nucleotide, which is consistently secured by hydrogen bonds within the pocket formed by residues M91, F93, and N9.

In contrast, when we examined the M2 simulation, we observed the most transient and less stable protein-RNA interactions, characterized by the lowest contact occupancy. We showed in the structural representation of the entire simulation that in the M2 trajectory, the RRM2 domain moves away from the binding interface, despite the RNA remaining bound to RRM1. This explains the less stable and more transient contacts observed in the RRM2 region of the analysis.

To analyze if RNA binding changes when the domains are separated, we performed MD simulations of the individual RRM1-RNA and RRM2-RNA complexes. We observed a significant decrease in stability of the core RRM-RNA interactions in both complexes, with interactions becoming more transient compared to the complete DND1-RNA complex.

From the RRM1-RNA simulations, we find that the main interaction of A4 with F61 remained stable in both M1 and M2 simulations, though this contact is present at a lower occupancy in M3. Given that the stabilizing effect of RRM2 on U6 has very low occupancy in the M2 simulation, RRM1 compensated by forming a new binding pocket around U5, involving residues R88, M90, F100, and Y102. Furthermore, in the M2 simulation the stable interactions with C1 are in two distinct regions (R64, L65 and N97, R98, G99). However, in the M3 simulation there is a modified interface: the A4 stacking on F61 is lost, yet the stable interaction with F100 is maintained. Furthermore, G8 is bound by M91, T92, and F93 (Figure S5 A). We also observe additional stable contacts around U7, surrounded by V36, N37, G38, and Q39.

In the simulations of the RRM2-RNA complex, there are fewer stable RRM-RNA interactions compared to the RRM1-RNA complex. The RNA did not form a stable binding interface in either M1 or M2 simulations, the RRM2-RNA form many interactions with low occupancy, this shows a transient binding. However, in the M3 simulation, RRM2-RNA complex has a defined binding interface marked by several interactions which were not present in the NMR structure. U5 and U6 were anchored in this interface with U5 stably bound by stacking interactions with W215 (Figure S5 B). Neither in the NMR structure, nor in the other simulations W215 is surface accessible, but it is buried inside RRM2 between the beta sheet and the alpha helix in the M1 and M2 systems, forming hydrogen bonds with H189 and K217.

Finally, U6 establishes stable contacts with M194 and K197. Our contact analysis indicates the cooperative binding of the tandem RRM domains (RRM1 and RRM2). This cooperation establishes a stable binding interface that persists despite the intrinsic flexibility observed within the DND1-RNA complex. Furthermore, we identified novel interactions that may serve as potential binding interfaces, suggesting that DND1 facilitates broad RNA recognition by allowing the two RRM domains to adopt multiple relative orientations.

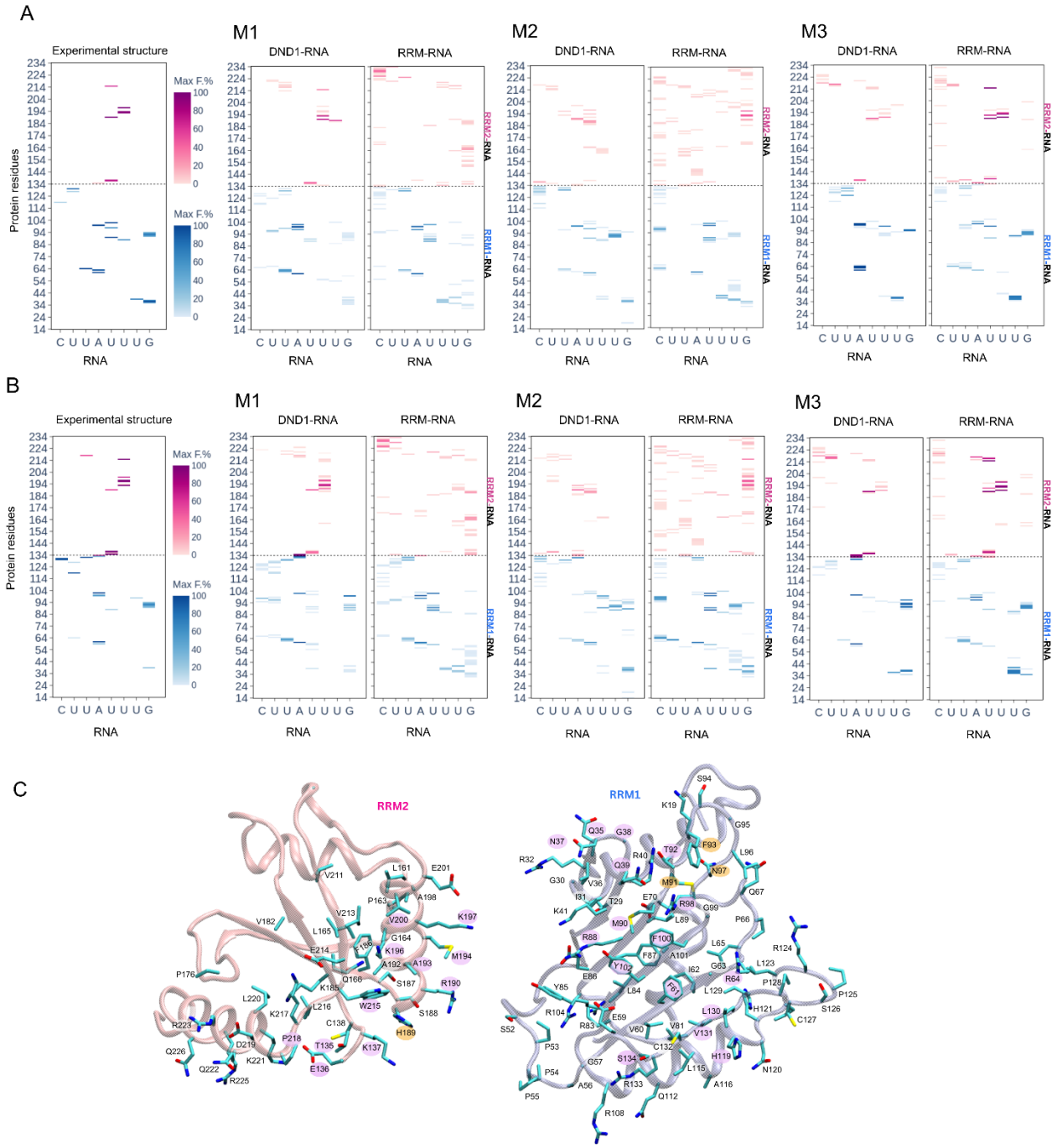

Figure 7. Contact analysis of the tandem RRM DND1-RNA complex compared to the RRM1-RNA and RRM2-RNA complexes. (A) Heatmaps of the protein to RNA backbone interactions (non-specific). (B) Heatmaps of the protein to RNA base interactions (sequence-specific). The first heatmap from the left shows the native contacts determined from the experimental NMR structure (average of ensemble from PDB: 7Q4L). All heatmaps are split horizontally based on the RRM1 (blue) and RRM2 (pink) residues. (C) Structural snapshot showing all residues involved in the

interaction, highlighting experimental contacts in purple and new potential binding residues identified in simulations in yellow.

Discussion

We found that the DND1-RNA complex displays high conformational plasticity in MD simulations, deviating significantly from the experimentally determined structure (PDB-ID: 7Q4L) (Duszczyk et al., 2022). The differences are mostly in the relative orientation of the two RRM motifs. The conformations sampled in the three independent simulations are different, suggesting that the simulation times are insufficient to achieve converged sampling of the inter-domain motion. Nevertheless, the three replicas per system allowed us to explore the dynamics involved extensively. The simulations did show similarities in terms of protein-RNA interactions, especially for those that define the core specificity of DND1. This indicates that the variability observed among the independent simulations, particularly the changing in the relative orientation of the two RRM domains, showcases a dynamic protein-RNA interface which may allow multiple RRM-RRM arrangements while maintaining the core RNA binding features. Notably, AF3 also predicts a different tandem RRM-RNA binding configuration than that in the NMR structure, providing further evidence for the conformational plasticity of this complex.

This plasticity may be specific for tandem RRM motifs recognizing RNA in a non-canonical manner [18], without involving the main β-sheet surfaces of both RRMs in the interaction. Or it may depend on the structure and length of the linker connecting the two RRMs which differs in tandem RRM containing proteins [14]. While the conformational flexibility of tandem RRMs is often linked to long, unstructured inter-domain linkers (e.g., in SRF1 binding;[19]), DND1 presents a structural paradox. It features a notably short, four-residue inter-domain linker, and its C-terminal RRM2 is non-canonical yet still crucial for RNA binding. As a key regulator, DND1 must bind long RNA sequences and facilitate protein-protein interactions [20].

Our simulations highlight that the DND1-RNA system maintains significant conformational plasticity despite the short linker and non-canonical RRM2. This inherent flexibility may be involved in its biological role, enabling DND1 to adapt its structure to various interactions. This finding is supported by a new crystal structure of the ternary DND1-RNA-NANOS3 complex (preprint [39]) which presents a different inter-domain orientation of the two RRMs compared to the original DND1-RNA complex structure (PDB: 7Q4L) [18]. In light of this evidence, our findings underscore that the conformational plasticity of tandem RRMs is not solely dependent on canonical structure or linker length, but is a fundamental mechanism allowing DND1 to adapt to binding other proteins in diverse regulatory processes.

The mechanism of high-affinity RNA recognition by DND1 relies on the cooperative binding of its tandem RRMs. Previous studies demonstrated that the maximum binding affinity is achieved only when both RRM domains are engaged [18,40]. In the case of DND1's cooperative model, the RRM1 domain functions as the main binding interface, while the RRM2 domain serves as a stabilizing anchor.

In our RRM1-RNA simulations the RNA remained stably bound even in the absence of RRM2, confirming RRM1's intrinsic capacity for high-affinity recognition. Specifically, in the RRM1-RNA simulations we identified new binding pockets accommodating the U5 and G8 nucleotide. This underscores RRM1's role as the initial, flexible docking site. The linker connecting the two RRM domains appears to exert minimal influence on the core binding affinity. This observation aligns with previous experimental data showing that a mutation of the linker does not reduce overall RNA binding [18].

The RRM2 domain, while contributing to the final stability, likely functions primarily as a cooperative trap for the RNA. Previous mutational study targeting the "unusual RNA-binding pocket" of RRM2 (K197A and W215F variants) resulted in significantly weaker binding, but did not completely abolish it, suggesting that these single mutations only partially disrupt the pocket[18]. In our DND1-RNA and RRM2-RNA simulations, the interaction Of the RNA with H189, stabilized the U5 position at the interface, suggesting a slightly different overall binding geometry compared to the experimental NMR structure [18]. The RRM2-RNA complex adopted multiple non-canonical binding geometries. In one simulation, the W215 residue stacked on U5, showcasing a potential, transient RRM2 recognition mode via an aromatic stacking interaction [41] while in a different simulation the RNA dissociated from RRM2. These findings reflect experimental data which shows that RRM2 does not show detectable binding to the RNA experimentally [18]. This behavior of RRM2 is consistent with that observed in other RRM proteins, such as the SRSF1 pseudo-RRM, which utilize α-helices or non-canonical motifs for transient binding.

These data suggest a model of cooperative RNA binding driven by a sequential engagement mechanism: the RNA initially engages the highly adaptable RRM1 domain in a canonical fashion, and the RRM2 domain reorients and converges toward RRM1, trapping the RNA between the two domains. This proposed enclosure mechanism is confirmed by our SASA calculations, which show a reduced accessibility for both RRM domains upon complex formation.

In such a dynamic mechanism it is plausible that the interaction between DND1 and its target RNA proceeds via a hybrid mechanism, combining elements of conformational selection and induced fit. The initial engagement is likely achieved through conformational selection, as the RRM1 domain binds using a pre-established conformation to an RNA conformation which is also sampled by the free RNA. Then the RRM2 domain reorients and converges towards RRM1 via an induced fit mechanism, forming an enclosure mechanism that traps the RNA and locks the domains into a stable complex.

The accuracy with which the simulations can predict such a mechanism depends on the force field parameters used. Historically, RNA force fields suffered from inaccuracies in describing structural ensembles of single stranded RNA. Conventional non-polarizable force field models like AMBER and CHARMM often overestimate electrostatic forces. This can lead to overly stable and compact complexes in the simulation, which may mask genuine conformational plasticity. While polarizable models may offer increased accuracy, and AMOEBA is demonstrated as a viable

option for studying protein-RNA systems [42], Baltrukevich and Bartos ultimately conclude that no single force field consistently outperforms others, suggesting no perfect solution for MD force field selection [43].

The accurate modeling of RNA is fundamentally challenged by its high conformational flexibility and requires precise force field parameterization to prevent computational artifacts such as unintended structural deviations and the formation of non-native loop conformations [44–47]. This difficulty is underscored by the existence of advanced force field alternatives, such as those incorporating NBfix corrections specifically designed to mitigate the collapse of single-stranded RNA [48].

We used the AMBER OL3 force field [35] for RNA coupled with the 4-point OPC (Optimal Point Charge) water model [33]. This combination is widely regarded as a robust and reliable benchmark for the simulation of nucleic acids [47,49]. Interestingly, with this combination we did not observe the collapsing of the RNA into compact structure as reported previously. [50,51]

The ionic conditions were carefully chosen to reproduce the protocol used to generate the NMR structure[18] which did not contain Mg^{2+}. While the inclusion of Mg^{2+} ions is frequently considered in RNA simulations [52,53], accurately modeling the properties of divalent ions remains inherently difficult. For this reason, Mg^{2+} inclusion is generally recommended only when its binding site is definitively known [47].

Previous MD simulation studies on protein-RNA interactions consistently highlight the inherent challenge of accurately modeling these highly dynamic systems and the flexibility of their binding mechanisms. For instance, increased flexibility and a broader range of binding modes were observed in MD simulations of the single-domain FUS protein in complex with a stem-loop RNA structure [54]. Similarly, an MD study examining the tandem RRM protein TDP-43 binding RNA showed a stable complex, but with differences in the binding mode compared to experimental data [55]. These examples underscore the critical point that MD simulations are complementary to structural experimental techniques like NMR or X-ray crystallography. By revealing the dynamic mechanism of these interactions, the simulations bring essential new information that static experimental structures cannot provide.

Additional MD simulations with different protocols may help in the thorough assessment of the force fields for such dynamic RNA based systems. Moreover, MD simulations of a tandem RRM proteins with canonical and non-canonical binding patterns in the future could provide a robust comparison platform for decoding the dynamics of tandem RRM-RNA interactions. This could open the door for future design of RRM containing proteins with special RNA binding features and for targeting tandem RRM proteins in disease.

Data Availability Statement

The MD simulations data with input and output files are provided at https://zenodo.org/records/17940554, https://zenodo.org/records/17940953, and https://zenodo.org/records/17944396

Acknowledgments

The Cojocaru group (https://cojocarulab.eu) is part of the Doctoral School in Integrative Biology of the Babes-Bolyai University and is supported by the Romanian Research Council (UEFISCDI), grant number PN-IV-P1-PCE-2023-1458/45PCE/08.01.2025. RGV is funded by the ministry of education of Romania. We thank Alexandre Bonvin and the Computational Structural Biology group at Utrecht University (https://bonvinlab.org) for support, feed-back and discussion. Vlad Cojocaru thanks Hans Schöler for continuous support and the Max Planck Computing and Data Facility (https://www.mpcdf.mpg.de/) for computer resources.

References

(1) Fierro-Monti, I. RBPs: An RNA Editor's Choice. *Front. Mol. Biosci.* **2024**, *11*. https://doi.org/10.3389/fmolb.2024.1454241.

(2) Corley, M.; Burns, M. C.; Yeo, G. W. How RNA-Binding Proteins Interact with RNA: Molecules and Mechanisms. *Mol. Cell* **2020**, *78*, 9–29. https://doi.org/10.1016/j.molcel.2020.03.011.

(3) Shotwell, C. R.; Cleary, J. D.; Berglund, J. A. The Potential of Engineered Eukaryotic RNA-Binding Proteins as Molecular Tools and Therapeutics. *Wiley Interdiscip. Rev. RNA* **2020**, *11*, e1573. https://doi.org/10.1002/wrna.1573.

(4) Varani, G.; Nagai, K. RNA Recognition by RNP Proteins during RNA Processing. *Annu. Rev. Biophys. Biomol. Struct.* **1998**, *27*, 407–445. https://doi.org/10.1146/annurev.biophys.27.1.407.

(5) Chen, Y.; Varani, G. Protein Families and RNA Recognition. *FEBS J.* **2005**, *272*, 2088–2097. https://doi.org/10.1111/j.1742-4658.2005.04650.x.

(6) Gerstberger, S.; Hafner, M.; Tuschl, T. A Census of Human RNA-Binding Proteins. *Nat. Rev. Genet.* **2014**, *15*, 829–845. https://doi.org/10.1038/nrg3813.

(7) Cléry, A.; Blatter, M.; Allain, F. H. T. RNA Recognition Motifs: Boring? Not Quite. *Curr. Opin. Struct. Biol.* **2008**, *18*, 290–298. https://doi.org/10.1016/j.sbi.2008.04.002.

(8) Ding, J.; Hayashi, M. K.; Zhang, Y.; Manche, L.; Krainer, A. R.; Xu, R. M. Crystal Structure of the Two-RRM Domain of HnRNP A1 (UP1) Complexed with Single-Stranded Telomeric DNA. *Genes Dev.* **1999**, *13*, 1102–1115. https://doi.org/10.1101/gad.13.9.1102.

(9) Conte, M. R.; Grüne, T.; Ghuman, J.; Kelly, G.; Ladas, A.; Matthews, S.; Curry, S. Structure of Tandem RNA Recognition Motifs from Polypyrimidine Tract Binding Protein Reveals Novel Features of the RRM Fold. *EMBO J.* **2000**, *19*, 3132–3141. https://doi.org/10.1093/emboj/19.12.3132.

(10) Nagai, K.; Oubridge, C.; Jessen, T. H.; Li, J.; Evans, P. R. Crystal Structure of the RNA-Binding Domain of the U1 Small Nuclear Ribonucleoprotein A. *Nature* **1990**, *348*, 515–520. https://doi.org/10.1038/348515a0.

(11) Maris, C.; Dominguez, C.; Allain, F. H. T. The RNA Recognition Motif, a Plastic RNA-Binding Platform to Regulate Post-Transcriptional Gene Expression. *FEBS J.* **2005**, *272*, 2118–2131. https://doi.org/10.1111/j.1742-4658.2005.04653.x.

(12) Oubridge, C.; Nagai, K.; Evans, P. R., et al. Crystal Structure at 1.92 Å Resolution of the RNA-Binding Domain of the U1A Spliceosomal Protein Complexed with an RNA Hairpin. *Nature* **1994**, *372*, 432–438. https://doi.org/10.1038/372432a0.

(13) Nowacka, M.; Boccaletto, P.; Jankowska, E.; Jarzynka, T.; Bujnicki, J. M.; Dunin-Horkawicz, S. RRMdb - An Evolutionary-Oriented Database of RNA Recognition Motif Sequences. *Database* **2019**, *2019*, bay148. https://doi.org/10.1093/database/bay148.

(14) Roca-Martínez, J.; Kang, H. S.; Sattler, M.; Vranken, W. Analysis of the Inter-Domain Orientation of Tandem RRM Domains with Diverse Linkers: Connecting Experimental with AlphaFold2 Predicted Models. *NAR Genom. Bioinf.* **2024**, *6*, lqae002. https://doi.org/10.1093/nargab/lqae002.

(15) Lukavsky, P. J.; Daujotyte, D.; Tollervey, J. R.; Ule, J.; Stuani, C.; Buratti, E.; Baralle, F. E.; Damberger, F. F.; Allain, F. H. T. Molecular Basis of UG-Rich RNA Recognition by the Human Splicing Factor TDP-43. *Nat. Struct. Mol. Biol.* **2013**, *20*, 1443–1449. https://doi.org/10.1038/nsmb.2698.

(16) Sun, Y. T.; Shortridge, M. D.; Varani, G. A Small Cyclic β-Hairpin Peptide Mimics the Rbfox2 RNA Recognition Motif and Binds to the Precursor MiRNA 20b. *ChemBioChem* **2019**, *20*, 931–939. https://doi.org/10.1002/cbic.201800645.

(17) Wang, X.; Tanaka Hall, T. M. Structural Basis for Recognition of AU-Rich Element RNA by the HuD Protein. *Nat. Struct. Biol.* **2001**, *8*, 141–145. https://doi.org/10.1038/84131.

(18) Duszczyk, M. M.; Wischnewski, H.; Kazeeva, T.; Arora, R.; Loughlin, F. E.; von Schroetter, C.; Pradère, U.; Hall, J.; Ciaudo, C.; Allain, F. H. T. The Solution Structure of Dead End Bound to AU-Rich RNA Reveals an Unusual Mode of Tandem RRM-RNA Recognition

Required for MRNA Regulation. *Nat. Commun.* **2022**, *13*, 5849. https://doi.org/10.1038/s41467-022-33552-x.

(19) De Silva, N. I. U.; Fargason, T.; Zhang, Z.; Wang, T.; Zhang, J. Inter-Domain Flexibility of Human Ser/Arg-Rich Splicing Factor 1 Allows Variable Spacer Length in Cognate RNA's Bipartite Motifs. *Biochemistry* **2022**, *61*, 2922–2932. https://doi.org/10.1021/acs.biochem.2c00565.

(20) Gross-Thebing, T.; Raz, E. Dead End and Detour: The Function of the RNA-Binding Protein Dnd in Posttranscriptional Regulation in the Germline. In *Curr. Top. Dev. Biol.*; Academic Press Inc., **2020**; Vol. 140, pp 181–208. https://doi.org/10.1016/bs.ctdb.2019.12.003.

(21) Gross-Thebing, T.; Yigit, S.; Pfeiffer, J.; Reichman-Fried, M.; Bandemer, J.; Ruckert, C.; Rathmer, C.; Goudarzi, M.; Stehling, M.; Tarbashevich, K.; Seggewiss, J.; Raz, E. The Vertebrate Protein Dead End Maintains Primordial Germ Cell Fate by Inhibiting Somatic Differentiation. *Dev. Cell* **2017**, *43*, 704-715.e5. https://doi.org/10.1016/j.devcel.2017.11.019.

(22) Weidinger, G.; Rg Stebler, J.; Slanchev, K.; Dumstrei, K.; Wise, C.; Lovell-Badge, R.; Thisse, C.; Thisse, B.; Raz, E. Dead End, a Novel Vertebrate Germ Plasm Component, Is Required for Zebrafish Primordial Germ Cell Migration and Survival Results and Discussion Zebrafish Dead End RNA Is a Component of the Germ Plasm and Is Specifically Expressed in Primordial Germ Cells. *Curr. Biol.* **2003**, *13*, 1429–1434. https://doi.org/10.1016/S1097-276.

(23) Faraji, H.; Banakar, F.; Sadri, A.; Ebrahim-Habibi, A. Dead-End Protein Expression, Function, and Mutation in Cancer: A Systematic Review. *Mol. Biol. Rep.* **2025**, *52*, 291. https://doi.org/10.1007/s11033-025-10325-5.

(24) Zhang, Y.; Li, Y.; Chachad, D.; Liu, B.; Godavarthi, J. D.; Williams-Villalobo, A.; Lasisi, L.; Xiong, S.; Matin, A. In Silico Analysis of DND1 and Its Co-Expressed Genes in Human Cancers. *Biochem. Biophys. Rep.* **2022**, *29*, 101206. https://doi.org/10.1016/j.bbrep.2022.101206.

(25) Wang, Z.; Yu, H.; Gu, Z. RNA-Binding Proteins DND1 and NANOS3 Cooperatively Suppress the Entry of Germ Cell Lineage. *Nat. Commun.* **2025**, *16*, 4792. https://doi.org/10.1038/s41467-025-57490-6.

(26) Zhang, Y.; Li, Y.; Chachad, D.; Liu, B.; Godavarthi, J. D.; Williams-Villalobo, A.; Lasisi, L.; Xiong, S.; Matin, A. In Silico Analysis of DND1 and Its Co-Expressed Genes in Human Cancers. *Biochem. Biophys. Rep.* **2022**, *29*, 101206. https://doi.org/10.1016/j.bbrep.2022.101206.

(27) Yang, Y.; Li, J.; Wei, C. Circular RNA CircFCHO2(Hsa_circ_0002490) Promotes the Proliferation of Melanoma by Directly Binding to DND1. *Cell Biol. Toxicol.* **2024**, *40*, 9. https://doi.org/10.1007/s10565-024-09851-y.

(28) Abramson, J.; Adler, J.; Dunger, J. Accurate Structure Prediction of Biomolecular Interactions with AlphaFold 3. *Nature* **2024**, *630*, 493–500. https://doi.org/10.1038/s41586-024-07487-w.

(29) Janin, J. L.; Henrick, K.; Moult, J.; Eyck, L. Ten; Sternberg, M. J. E.; Vajda, S.; Vakser, I.; Wodak, S. J. CAPRI: A Critical Assessment of PRedicted Interactions; **2003**. http://capri.ebi.ac.uk/.

(30) Giulini, M.; Reys, V.; Teixeira, J. M. C.; Jiménez-García, B.; Honorato, R. V.; Kravchenko, A.; Xu, X.; Versini, R.; Engel, A.; Verhoeven, S.; Bonvin, A. M. J. J. HADDOCK3: A Modular and Versatile Platform for Integrative Modeling of Biomolecular Complexes. *J. Chem. Inf. Model.* **2025**, *65*, 7315–7324. https://doi.org/10.1021/acs.jcim.5c00969.

(31) Webb, B.; Sali, A. Comparative Protein Structure Modeling Using MODELLER. *Curr. Protoc. Bioinform.* **2016**, *2016*, 5.6.1-5.6.37. https://doi.org/10.1002/cpbi.3.

(32) UniProtKB: Dead end protein homolog 1 (Human). Accession Q8IYX4. UniProt Consortium, *https://www.uniprot.org/uniprotkb/Q8IYX4/entry* (Accessed: December 15, 2025).

(33) Izadi, S.; Anandakrishnan, R.; Onufriev, A. V. Building Water Models: A Different Approach. *J. Phys. Chem. Lett.* **2014**, *5*, 3863–3871. https://doi.org/10.1021/jz501780a.

(34) Tian, C.; Kasavajhala, K.; Belfon, K. A. A.; Raguette, L.; Huang, H.; Migues, A. N.; Bickel, J.; Wang, Y.; Pincay, J.; Wu, Q.; Simmerling, C. Ff19SB: Amino-Acid-Specific Protein Backbone Parameters Trained against Quantum Mechanics Energy Surfaces in Solution. *J. Chem. Theory Comput.* **2020**, *16*, 528–552. https://doi.org/10.1021/acs.jctc.9b00591.

(35) Zgarbová, M.; Otyepka, M.; Šponer, J.; Mládek, A.; Banáš, P.; Cheatham, T. E.; Jurečka, P. Refinement of the Cornell et al. Nucleic Acids Force Field Based on Reference Quantum Chemical Calculations of Glycosidic Torsion Profiles. *J. Chem. Theory Comput.* **2011**, *7*, 2886–2902. https://doi.org/10.1021/ct200162x.

(36) Case, D. A.; Aktulga, H. M.; Belfon, K.; Cerutti, D. S.; Cisneros, G. A.; Cruzeiro, V. W. D.; Forouzesh, N., et al. AmberTools. *J. Chem. Inf. Model.* **2023**, *63*, 6183–6191. https://doi.org/10.1021/acs.jcim.3c01153.

(37) Phillips, J. C.; Hardy, D. J.; Maia, J. D. C.; Stone, J. E.; Ribeiro, J. V.; Bernardi, R. C.; Buch, R., et al. Scalable Molecular Dynamics on CPU and GPU Architectures with NAMD. *J. Chem. Phys.* **2020**, *153*, 044130. https://doi.org/10.1063/5.0014475.

(38) Shao, J.; Tanner, S. W.; Thompson, N.; Cheatham, T. E. Clustering Molecular Dynamics Trajectories: 1. Characterizing the Performance of Different Clustering Algorithms. *J. Chem. Theory Comput.* **2007**, *3*, 2312–2334. https://doi.org/10.1021/ct700119m.

(39) Suzawa, M.; Qiu, C.; Polash, A. H.; Yamaji, M.; Jacob, A. A.; Horikawa, W.; Farroha, E. M.; Barua, M.; Feng, X.; Liu, C.; Williams, J. G.; Randazzo, D.; Sartorelli, V.; Valkov, E.;

Yamaji, M.; Hall, T. M. T.; Hafner, M. The DND1–NANOS3 Complex Shapes the Primordial Germ Cell Transcriptome via a Heptanucleotide Sequence in MRNA 3′ UTRs. **2025**. https://doi.org/10.1101/2025.09.25.678639.

(40) Ozguney, B.; Mohanty, P.; Mittal, J. RNA Binding Tunes the Conformational Plasticity and Intradomain Stability of TDP-43 Tandem RNA Recognition Motifs. *Biophys. J.* **2024**, *123*, 3844–3855. https://doi.org/10.1016/j.bpj.2024.09.031.

(41) Cléry, A.; Sinha, R.; Anczuków, O.; Corrionero, A.; Moursy, A.; Daubner, G. M.; Valcárcel, J.; Krainer, A. R.; Allain, F. H. T. Isolated Pseudo-RNA-Recognition Motifs of SR Proteins Can Regulate Splicing Using a Noncanonical Mode of RNA Recognition. *Proc. Natl. Acad. Sci. U. S. A.* **2013**, *110*, 12690–12695. https://doi.org/10.1073/pnas.1303445110.

(42) Jing, Z.; Ren, P. Molecular Dynamics Simulations of Protein RNA Complexes by Using an Advanced Electrostatic Model. *J. Phys. Chem. B* **2022**, *126*, 7343–7353. https://doi.org/10.1021/acs.jpcb.2c05278.

(43) Baltrukevich, H.; Bartos, P. RNA-Protein Complexes and Force Field Polarizability. *Front. Chem.* **2023**, *11*. https://doi.org/10.3389/fchem.2023.1217506.

(44) Bernetti, M.; Bussi, G. Integrating Experimental Data with Molecular Simulations to Investigate RNA Structural Dynamics. *Curr. Opin. Struct. Biol.* **2023**, *78*, 102503. https://doi.org/10.1016/j.sbi.2022.102503.

(45) Liebl, K.; Zacharias, M. The Development of Nucleic Acids Force Fields: From an Unchallenged Past to a Competitive Future. *Biophys. J.* **2023**, *122*, 2841–2851. https://doi.org/10.1016/j.bpj.2022.12.022.

(46) Muscat, S.; Martino, G.; Manigrasso, J.; Marcia, M.; De Vivo, M. On the Power and Challenges of Atomistic Molecular Dynamics to Investigate RNA Molecules. *J. Chem. Theory Comput.* **2024**, *20*, 6831–6845. https://doi.org/10.1021/acs.jctc.4c00773.

(47) Mlýnský, V.; Kührová, P.; Pykal, M.; Krepl, M.; Stadlbauer, P.; Otyepka, M.; Banáš, P.; Šponer, J. Can We Ever Develop an Ideal RNA Force Field? Lessons Learned from Simulations of the UUCG RNA Tetraloop and Other Systems. *J. Chem. Theory Comput.* **2025**, *21*, 4183–4202. https://doi.org/10.1021/acs.jctc.4c01357.

(48) Mlýnský, V.; Kührová, P.; Stadlbauer, P.; Krepl, M.; Otyepka, M.; Banáš, P.; Šponer, J. Simple Adjustment of Intranucleotide Base-Phosphate Interaction in the OL3 AMBER Force Field Improves RNA Simulations. *J. Chem. Theory Comput.* **2023**, *19*, 8423–8433. https://doi.org/10.1021/acs.jctc.3c00990.

(49) Bottaro, S.; Bussi, G.; Kennedy, S. D.; Turner, D. H.; Lindorff-Larsen, K. Conformational Ensembles of RNA Oligonucleotides from Integrating NMR and Molecular Simulations. *Sci. Adv.* **2018**, *4*, eaar8521. https://doi.org/10.1126/sciadv.aar8521.

(50) Mráziková, K.; Mlýnský, V.; Kührová, P.; Pokorná, P.; Kruse, H.; Krepl, M.; Otyepka, M.; Banáš, P.; Šponer, J. UNCG RNA Tetraloop as a Formidable Force-Field Challenge for MD Simulations. **2020**. https://doi.org/10.1101/2020.07.27.223826.

(51) Šponer, J.; Bussi, G.; Krepl, M.; Banáš, P.; Bottaro, S.; Cunha, R. A.; Gil-Ley, A.; Pinamonti, G.; Poblete, S.; Jurečka, P.; Walter, N. G.; Otyepka, M. RNA Structural Dynamics as Captured by Molecular Simulations: A Comprehensive Overview. *Chem. Rev.* **2018**, *118*, 4177–4338. https://doi.org/10.1021/acs.chemrev.7b00427.

(52) Fischer, N. M.; Polêto, M. D.; Steuer, J.; van der Spoel, D. Influence of Na^{2+} and Mg^{2+} Ions on RNA Structures Studied with Molecular Dynamics Simulations. *Nucleic Acids Res.* **2018**, *46*, 4872–4882. https://doi.org/10.1093/nar/gky221.

(53) Viegas, R. G.; Sinha, A.; Mainan, A.; Sanbonmatsu, K. Y.; Onuchic, J. N.; Roy, S.; Leite, V. B. P. Critical Role of Mg^{2+} Ions in RNA Folding Transitions: Anchoring the A-Minor Twist in the SAM-II Riboswitch. *J. Phys. Chem. B* **2025**, *129*, 9058–9067. https://doi.org/10.1021/acs.jpcb.5c02586.

(54) Pokorná, P.; Krepl, M.; Campagne, S.; Šponer, J. Conformational Heterogeneity of RNA Stem-Loop Hairpins Bound to FUS RNA Recognition Motif with Disordered RGG Tail Revealed by Unbiased Molecular Dynamics Simulations. **2022**. https://doi.org/10.1101/2022.08.16.504132.

(55) Donald Scott, D.; Mowrey, D.; Nagarajan, K.; Nair, A.; Khanna, M. Molecular Dynamics Simulation of TDP-43 RRM in the Presence and Absence of RNA. *J. Bioinf. Syst. Biol.* **2024**, *7*. https://doi.org/10.26502/jbsb.5107088.